J Fluoresc (2009) 19:623–629
DOI 10.1007/s10895-008-0453-8

ORIGINAL PAPER

Synthesis and Characterization of Monodispersed $SiO_2@Y_3Al_5O_{12}:Er^{3+}$ Core-Shell Particles

Cheng-Ning Xie · Zhong-Min Yang · Yan-Hui Sun

Received: 25 October 2008 / Accepted: 3 December 2008 / Published online: 23 December 2008

Abstract Submicron core-shell structure particles $SiO_2@Y_3Al_5O_{12}:Er^{3+}$, which silica spherical particles was coated with an yttrium aluminum garnet ($Y_3Al_5O_{12}$) layer doped with Er^{3+}, were prepared by the modified Pechini-Type sol-gel method for the first time. The structure and morphology of samples were detected by the X-ray powder diffraction (XRD) measurement, field emission scanning electron microscopy (FESEM) and transmission electron microscopy (TEM), respectively. The results indicate that well-crystallized garnet nanocrystallines were formed on the surface of the silica particles. The luminescent spectra in near infrared and visible region of the core-shell structured $SiO_2@Y_3Al_5O_{12}:Er^{3+}$ powders were also investigated and compared with those of the pure $Y_3Al_5O_{12}:Er^{3+}$ and the Er^{3+} doped silicate glass. The results show that mono-dispersed $SiO_2@Y_3Al_5O_{12}:Er^{3+}$ core-shell spherical particles with the near infrared, red and green luminescent emissions under the excitation of 980 nm laser diode have been successfully synthesized.

Keywords $Y_3Al_5O_{12}:Er^{3+}$ · Core-shell · Morphology · Luminescence

C.-N. Xie · Z.-M. Yang (✉)
Key Lab of Specially Functional Materials of Ministry of Education and Institute of Optical Communication Materials, South China University of Technology, Guangzhou 510641, People's Republic of China
e-mail: yangzm@scut.edu.cn

Y.-H. Sun
School of Environment and Chemistry, South China Normal University, Guangzhou 510006, People's Republic of China

Introduction

Erbium doped yttrium aluminum garnet ($Y_3Al_5O_{12}:Er^{3+}$) polycrystalline has a potential application in optical communication [1] and solid-state lasers [2–4] because of its good mechanical and thermal characteristics. The synthesis and spectroscopic investigation of $Y_3Al_5O_{12}:Er^{3+}$ has been carried out with growing interest [1–8]. However, it's still difficult to obtain the polycrystalline $Y_3Al_5O_{12}$ with an ideally spherical morphology, narrow size distribution and well-dispersed state. All of these features are beneficial to get high brightness and high resolution when the polycrystalline is used as phosphors in bio-probe researches. And they are also essential for obtaining high packing densities and low light scattering when the polycrystalline is used as the raw material of transparent ceramic sinter.

Nowadays, core-shell structure is becoming of growing interest for multipurpose applications [9–13]. This structure can keep the core away from the interaction with the surrounding medium and obtain specific morphology of the as-formed materials, which is suitable for fabricating the spherical morphology of $Y_3Al_5O_{12}$. A variety of approaches have been employed for the manufacture of core-shell structured materials, such as co-precipitation, layer-by-layer self-assembly, sol-gel process and so on. Of these methods the sol-gel process is a convenient technique to provide good mixing of starting materials and relatively low reaction temperature for more homogeneous products. Recently, a core-shell $SiO_2@Y_3Al_5O_{12}$ using the amorphous SiO_2 as core has been synthesized, but the $Y_3Al_5O_{12}$ shell prepared by the same method exhibits a large difference in the morphology reported in different literatures [14, 15]. Furthermore, the luminescent spectra of rare-earth ions is strongly affected by the crystal field around the rare-earth ions, which has not been discussed in these articles yet.

In the present work, $Y_3Al_5O_{12}:Er^{3+}$ polycrystalline coated on amorphous SiO_2 made by Stöber method [16] was synthesized by sol-gel method for the first time. Detailed characterizations for the structure, morphology, luminescent properties of the samples were investigated.

Experimental

Synthesis process of the samples

The highly monodispersed amorphous SiO_2 spheres with a size around 150 nm were prepared by the well-known Stöber method [16, 17]. The coating of $Y_3Al_5O_{12}:Er^{3+}$ layers on the SiO_2 spheres was synthesized by a modified Pechini type sol-gel process [14, 15, 18]. The dopant concentration of Er^{3+} was 2 at % in $Y_3Al_5O_{12}$. Briefly, proper amount of corresponding nitrates of Y^{3+}, Al^{3+} and Er^{3+} were firstly mixed into alcohol-water solution together according to the stoichiometry of $Y_3Al_5O_{12}$. And then the citric acid and polyethylene glycol (molecular weight = 10,000) were added. The molar ratio of metal ions to citric acid was 1:2. After the solution was stirred to form sol, the SiO_2 spheres were added. Then the suspension was stirred for another 4 h followed by centrifugation and dry. The powder samples obtained were annealed at 500°C. Above process was reapeated several times to increase the garnet amount. At last, the samples with different number of coating cycles were annealed at 1000°C for 5 h. For comparison, the rest solution was stirred to form a gel, and the gel was annealed with the same process to obtain pure $Y_3Al_5O_{12}:Er^{3+}$ powders.

Characterization

The X-ray diffraction (XRD) of as-prepared samples was performed on a Philips Model PW1,830 diffractometer using Cu $K_{\alpha 1}$ radiation. The morphology of the samples was observed using a field emission scanning electron microscope (FESEM, LEO 1530 VP) and transmission electron microscope (TEM, JEM-100CXII, 100 kV). The luminescent spectra of Er^{3+} ion were recorded at room temperature using a Triax320 fluorescence spectrometer (Jobin-Yvon Inc., France) with a 980-nm LD as the excitation source.

Results and discussion

Formation and morphological properties

Figure 1 shows the XRD patterns of bare SiO_2 (a), thrice-coated $SiO_2@Y_3Al_5O_{12}:Er^{3+}$ (b) and $Y_3Al_5O_{12}:Er^{3+}$ powders (c) as well as the standard data for $Y_3Al_5O_{12}$ (JCPDS No. 33-0040) as a reference, respectively. For SiO_2 directly formed from Stöber method (Fig. 1(a)), no diffraction peak is observed except for a broad band centered at $2\theta=22°$, which is identical with the standard XRD pattern for amorphous SiO_2 (JCPDS No. 29-0085, not presented). For $SiO_2@Y_3Al_5O_{12}:Er^{3+}$ particles, no characteristic diffraction peaks of $Y_3Al_5O_{12}$ appear when the coating cycle is less than twice, just as shown in Fig. 1(b). After the amorphous SiO_2 was coated two times, diffraction peaks belonging to the crystallized $Y_3Al_5O_{12}$ with cubic structure (space group: *Ia3d*) appear besides the broad band from amorphous SiO_2. No other phase is detected from the comparison of the diffraction patterns of the $Y_3Al_5O_{12}:Er^{3+}$ particles (Fig. 1(c)) with the standard data for $Y_3Al_5O_{12}$, indicating that no reaction occurs between the core and shell at the annealing temperature. However, the diffraction spectral bands considerably broaden, suggesting that the size of nanocrystallite would be small. Based on the Scherrer equation [19], the Scherrer Calculator program of X' PERT HightScore software is used to calculate the crystalline size of the samples. The average size of $Y_3Al_5O_{12}:Er^{3+}$ nanocrystallite coated on the SiO_2 spheres and pure $Y_3Al_5O_{12}:Er^{3+}$ powders are calculated to be 29 nm and 42 nm, respectively.

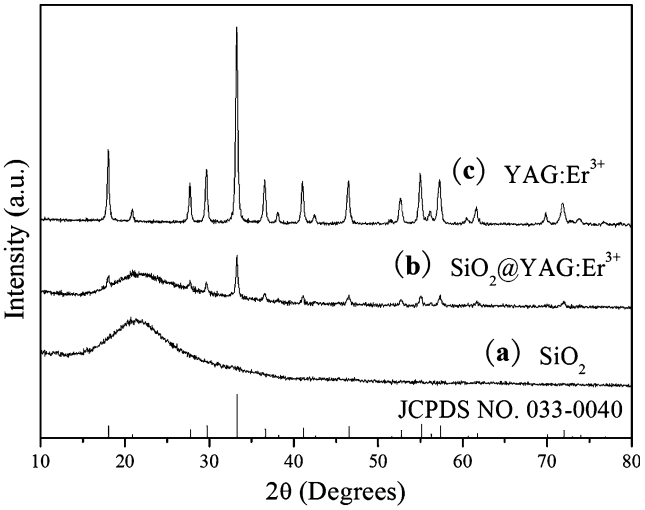

Fig. 1 XRD patterns of bare SiO_2 (**a**), thrice-coated $SiO_2@Y_3Al_5O_{12}:Er^{3+}$ (**b**) and $Y_3Al_5O_{12}:Er^{3+}$ particles (**c**) as well as the standard data for $Y_3Al_5O_{12}$ (JCPDS No. 033-0040) as a reference

Figure 2 shows the FESEM morphology of the as-synthesized amorphous SiO_2 (a), thrice-coated $SiO_2@Y_3Al_5O_{12}:Er^{3+}$ (b) and $Y_3Al_5O_{12}:Er^{3+}$ particles (c), respectively. From the Fig. 2(a), one can note that the diameter of bare SiO_2 spheres is keeping in a tiny range centered at about 150 nm without aggregation. After coated with $Y_3Al_5O_{12}:Er^{3+}$ thrice (Fig. 2(b)), the $SiO_2@Y_3Al_5O_{12}:Er^{3+}$ particles are still spherical and non-aggregated. Some irregular substance close to SiO_2 spheres or existing

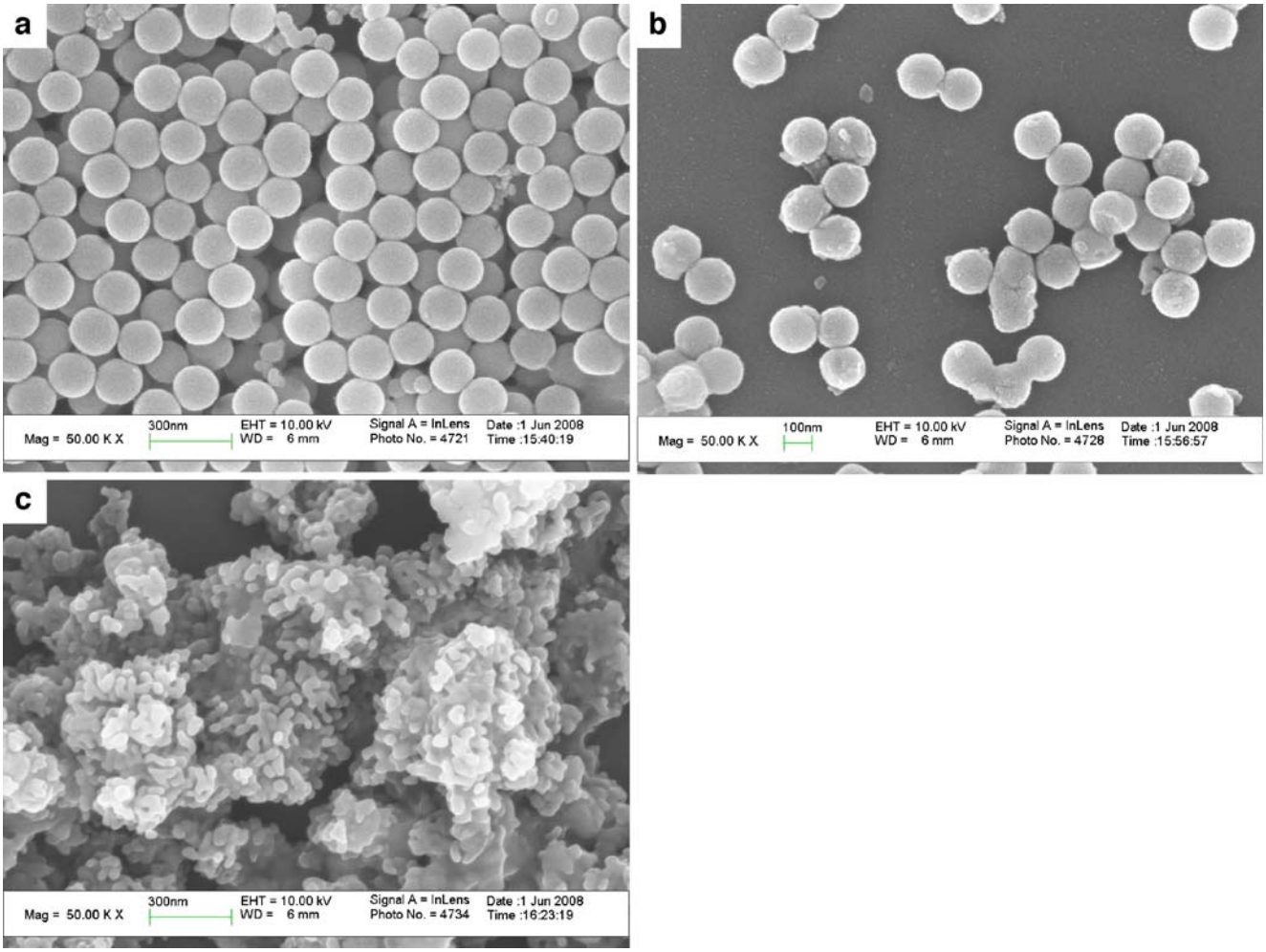

Fig. 2 FESEM micrographs of the as-formed amorphous SiO_2 (**a**), thrice-coated $SiO_2@Y_3Al_5O_{12}:Er^{3+}$ (**b**) and $Y_3Al_5O_{12}:Er^{3+}$ powders (**c**)

between SiO_2 spheres are observed, which is similar with the observation at [15]. The average diameter of these particles is slightly larger than the bare SiO_2 spheres, i.e., nearly 200 nm. The thickness of the coating layer is estimated to be 25 nm, which is comparative with the average crystal size of $Y_3Al_5O_{12}:Er^{3+}$ calculated from the Scherrer equation. This indicates that the $Y_3Al_5O_{12}:Er^{3+}$ materials can be applied to the surface of silica particles by sol-gel method. The pure $Y_3Al_5O_{12}:Er^{3+}$ powders (Fig. 2(c)) have an average size of about 40 nm, but aggregated severely.

In order to further observe the core-shell structure of $SiO_2@Y_3Al_5O_{12}:Er^{3+}$ particles, TEM technique is employed. Fig. 3 shows the TEM morphology of the as-formed amorphous SiO_2 (a) and the SiO_2 particles coated with $Y_3Al_5O_{12}:Er^{3+}$ twice (b) and thrice (c) with 100 kX magnification. For the bare amorphous SiO_2 (Fig. 3(a)), the diameter is 150 nm, which is the same as that observed from FESEM. Obviously, after functionalizing the silica cores with $Y_3Al_5O_{12}:Er^{3+}$ coating twice, the morphology of resulting $SiO_2@Y_3Al_5O_{12}:Er^{3+}$ in Fig. 3(b) still keeps spherical and non-aggregated, but the surface of the particles becomes rough. For the thrice-coated particles (Fig. 3(c)), a thin successive layer appears around the SiO_2 sphere obviously and has the thickness of about 25 nm, which agrees well with the estimation from the FESEM morphology of Fig 2(b).

Photoluminescence properties

Figure 4 and Fig. 5 show the downconversion photoluminescence spectra of the $SiO_2@Y_3Al_5O_{12}:Er^{3+}$ with different coating cycles and the spectral comparison with the $Y_3Al_5O_{12}:Er^{3+}$ powders and Er^{3+} doped silicate glass in near infrared (NIR) region, respectively. The Er^{3+} doped silicate glass was fabricated in our laboratory. It can be seen from Fig. 4 that the luminescence of all the samples has a strong peak at 1525 nm and some weak peaks centered at 1468, 1510, 1542, 1612, 1640 nm. All the peaks are assigned to the *f-f* transitions of Er^{3+} from $^4I_{13/2}$ to $^4I_{15/2}$.

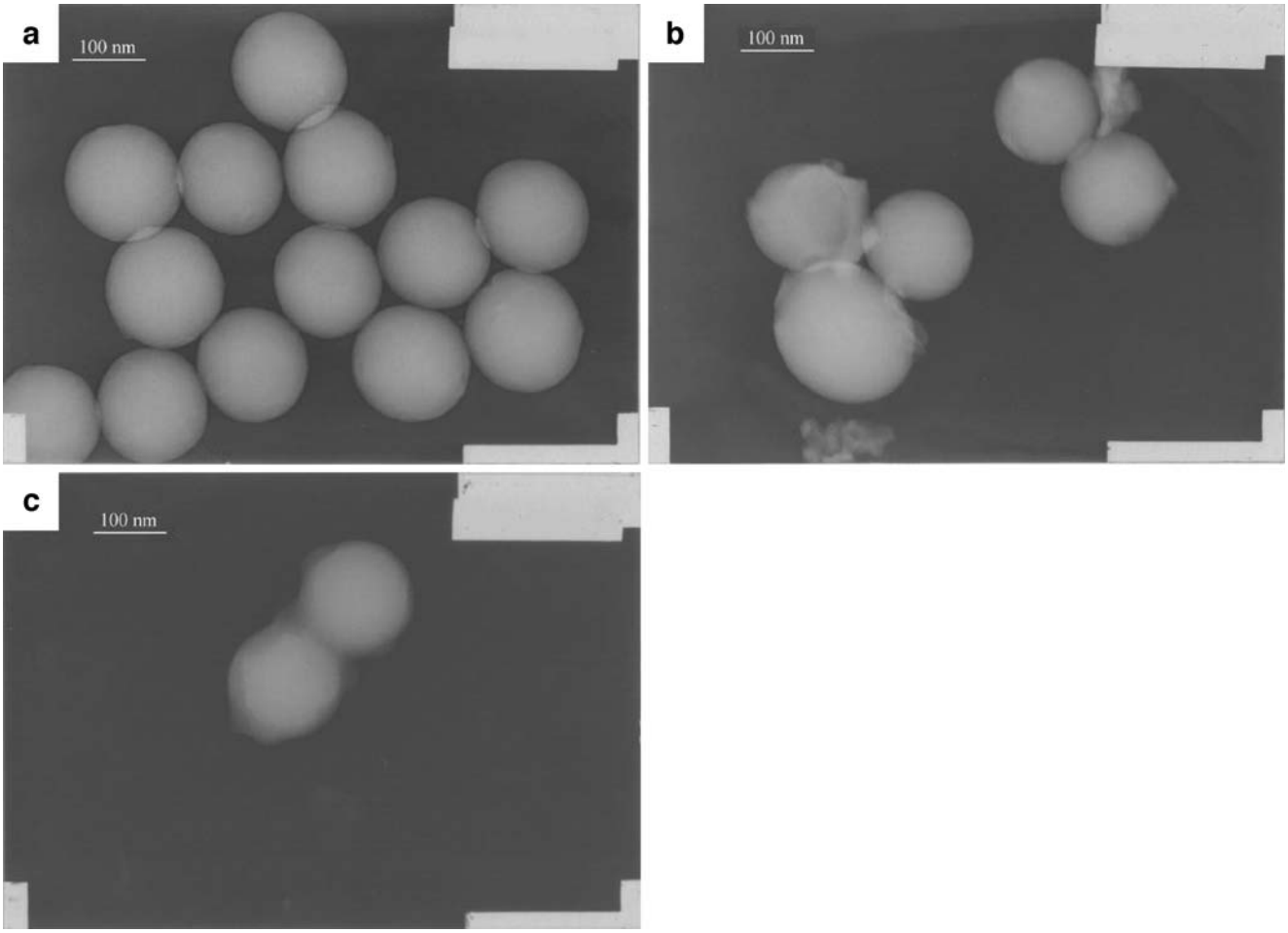

Fig. 3 TEM micrographs of the as-formed amorphous SiO_2 (**a**) and twice-coated $SiO_2@Y_3Al_5O_{12}:Er^{3+}$ (**b**) and thrice-coated $SiO_2@Y_3Al_5O_{12}:Er^{3+}$ (**c**) with 100 kX magnification

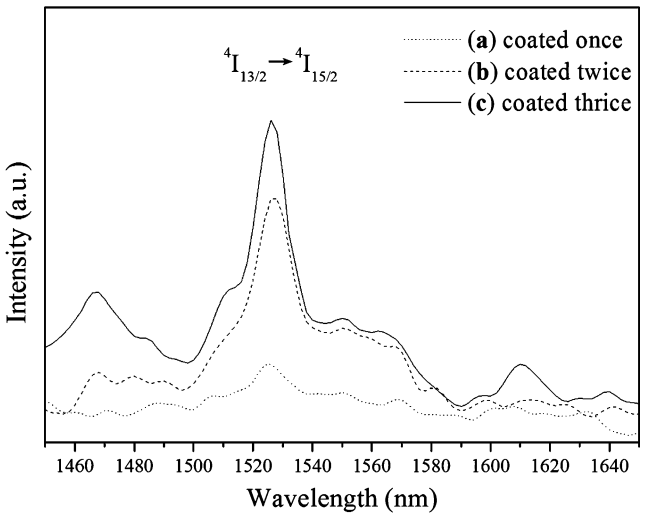

Fig. 4 Downconversion luminescent spectra of the $SiO_2@Y_3Al_5O_{12}:Er^{3+}$ with different coating cycles in near infrared region

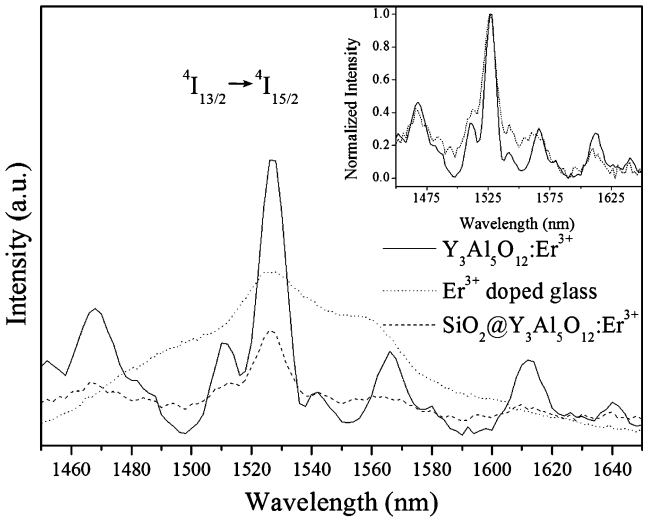

Fig. 5 Downconversion luminescent spectra of the $SiO_2@Y_3Al_5O_{12}:Er^{3+}$, $Y_3Al_5O_{12}:Er^{3+}$ powders and Er^{3+} doped glass in near infrared region. The normalization spectra of the $SiO_2@Y_3Al_5O_{12}:Er^{3+}$ and $Y_3Al_5O_{12}:Er^{3+}$ samples was shown in the inset

With 980-nm LD exciting, an Er^{3+} ion at the ground state $^4I_{15/2}$ absorbs one photon (GSA) and jumps to the $^4I_{11/2}$ level, then nonradiatively decays to the $^4I_{13/2}$ level. The excited Er^{3+} ion radiatively decays from the $^4I_{13/2}$ level to the ground state and one NIR photon is generated as shown in Fig. 6. Thanks to the degenerate-lift effect of crystal field, the levels $^4I_{15/2}$ and $^4I_{13/2}$ of Er^{3+} ions, which are in D2 symmetry of the garnet lattice, are split [3]. So in Fig. 4 one can see a series of NIR emissions with different peak values from the same transition of $^4I_{13/2} \rightarrow ^4 I_{15/2}$. Based on the level splitting of Er^{3+} ions in the $Y_3Al_5O_{12}$ crystal reported at [20], there should have 56 transitions from each sublevel of $^4I_{13/2}$ to that of $^4I_{15/2}$ with the emission wavelength ranging from 1454 nm to 1673 nm. Because the $^4I_{15/2}$ level has eight splitting sublevels and the $^4I_{13/2}$ level has seven splitting sublevels at low temperature. However, due to the thermal vibration of crystal lattice at room temperature, some transitions with approximate emission wavelength happen synchronously and makes the emission bands broaden in the present work.

The effect of the coating cycles on the intensity of luminescence is also shown in Fig. 4. For the sample coated once, the luminescence is still too weak to be observed. With the $Y_3Al_5O_{12}$ coating cycles increasing, the intensity of luminescence in NIR region is enhanced. It can be explained as follows: the increase of coating cycle thicken the coating layer from 0 nm to 25 nm (Fig. 3), which means more garnet is adhered to the surface of SiO_2. Moreover, the crystallization degree of the nanocrystallines is enhanced by the thicker coating layer, which makes the luminescence of Er^{3+} ions less disturbance from the interfacial effect of nanocrystals. So the intensity of luminescence shows an increasing trend with the coating cycles.

From Fig. 5, one can note that the emission pattern of the $SiO_2@Y_3Al_5O_{12}:Er^{3+}$ sample has a large difference from that of the Er^{3+} doped glass and is similar with that of the pure $Y_3Al_5O_{12}:Er^{3+}$ powders. In glass, the Er^{3+} ions are embedded in the disorder network structure, which makes the emission spectrum inhomogeneous broadening. Different from the glass, the spectrum of pure $Y_3Al_5O_{12}:Er^{3+}$ powders have finger patterns due to the ordered crystal structure. The $SiO_2@Y_3Al_5O_{12}:Er^{3+}$ sample shows the similar finger patterns, demonstrating that Er^{3+} ions of the core-shell material exist in an ordered structure. However, the emission intensity of core-shell sample is so weak compared with that of the pure $Y_3Al_5O_{12}:Er^{3+}$ powders. The inset of Fig. 5 shows the normalized spectra of the two samples. The pure $Y_3Al_5O_{12}:Er^{3+}$ powders has a slightly narrower peak width for the band centered at 1525 nm than that of the core-shell sample. It indicates that the former have higher symmetry of crystal field and Er^{3+} ions enter into the same lattice site. Moreover, Er^{3+} ions in the coating $Y_3Al_5O_{12}$ are effected by the size of the nanocrystal and surface energy and lattice sites, all of which broaden the emission peak. The integral intensity of the emission in NIR region of the two samples were also investigated. The integral intensity value is 0.08342 and 0.02674 for the pure $Y_3Al_5O_{12}:Er^{3+}$ powders and the core-shell sample, respectively. It's obvious that the value of the former is nearly four times that of the latter, suggesting that the pure $Y_3Al_5O_{12}:Er^{3+}$ powders can transform the excitation energy more efficiently than the core-shell sample.

Figure 7 and Fig. 8 show the upconversion spectra of the $SiO_2@Y_3Al_5O_{12}:Er^{3+}$ with different coating cycles and the spectral comparison with the $Y_3Al_5O_{12}:Er^{3+}$ powders and Er^{3+} doped silicate glass in visible region, respectively. As shown in Fig. 7, the spectra should be divided into three

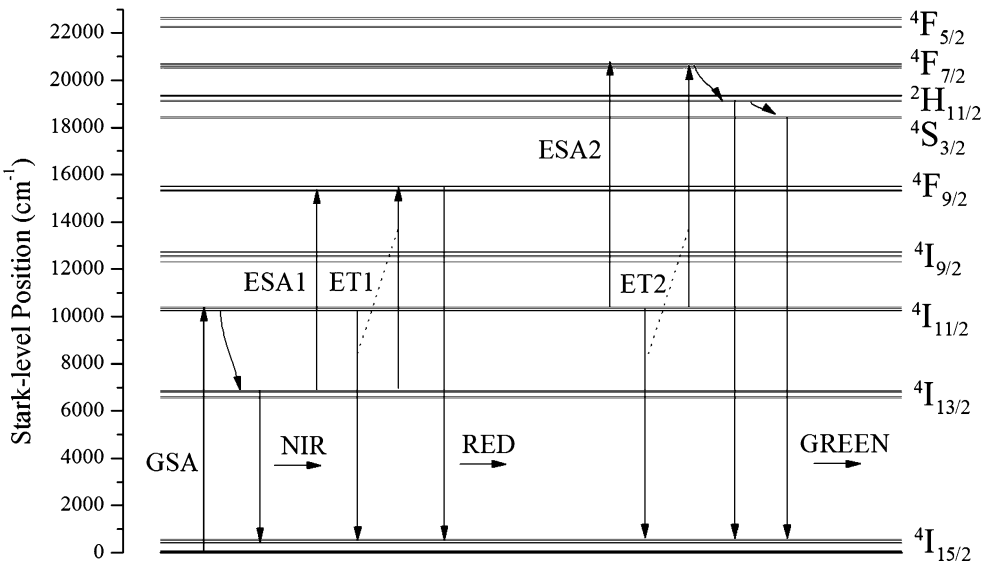

Fig. 6 The emission scheme of Er^{3+} in $Y_3Al_5O_{12}:Er^{3+}$

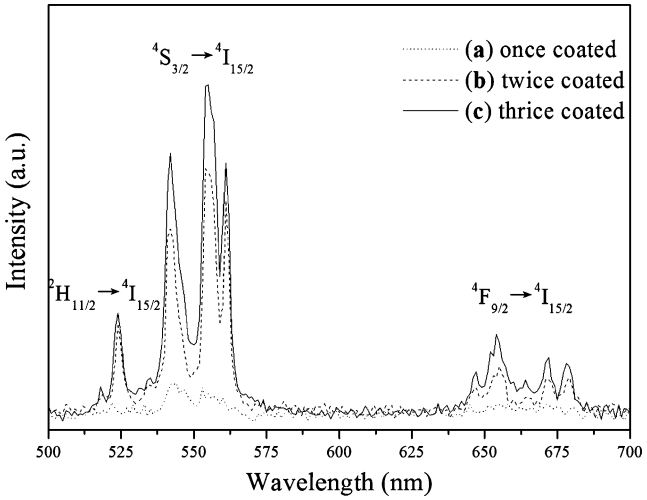

Fig. 7 Upconversion luminescent spectra of the $SiO_2@Y_3Al_5O_{12}:Er^{3+}$ with different coating cycles in visible region

parts: the $^4F_{9/2} \rightarrow {}^4I_{15/2}$ transition in the range from 640 nm to 685 nm stands for the red luminescence, the $^4S_{3/2} \rightarrow {}^4I_{15/2}$ transitions in the range from 530 nm to 570 nm and the $^4H_{11/2} \rightarrow {}^4I_{15/2}$ transitions in the range from 510 nm to 530 nm for the green luminescence, respectively. For the visible emission, the upconversion process is intensely affected by the excited-state absorption (ESA) and energy transfer (ET) processes [3, 4, 21]. Under the excitation of 980-nm LD there are four processes that mainly contribute to the upconversion emission, as depicted in Fig. 6:

$$\text{ESA1}: {}^4I_{13/2} + \text{one photon} \rightarrow {}^4F_{9/2}$$
$$\text{ESA}: {}^4I_{11/2} + \text{one photon} \rightarrow {}^4F_{7/2}$$
$$\text{ET1}: \left({}^4I_{13/2}, {}^4I_{11/2}\right) \rightarrow \left({}^4F_{9/2}, {}^4I_{15/2}\right)$$
$$\text{ET2}: \left({}^4I_{11/2}, {}^4I_{11/2}\right) \rightarrow \left({}^4F_{7/2}, {}^4I_{15/2}\right)$$

Make it detailed, the levels $^4I_{11/2}$ and $^4I_{13/2}$ are populated after the GSA process. Then the level $^4F_{9/2}$ is populated by the ESA 1 and ET 1 processes, while the levels $^2H_{11/2}$ is populated by the ESA 2 and ET 2 processes followed by nonradiative decay from the level $^4F_{7/2}$. A rapid thermal population between the levels $^2H_{11/2}$ and $^4S_{3/2}$ take place prior to the radiative transition. Radiative transitions from the levels $^4F_{9/2}$, $^2H_{11/2}$ and $^4S_{3/2}$ emit red and green light, respectively. Similar to NIR emission, all of the initial levels of emission are spilt by the degenerate-lift effect of crystal field and each specific transition has several emission peaks. There are five peaks located at 646 nm, 654 nm, 660 nm, 671 nm and 678 nm for red emission and five peaks located at 517 nm, 524 nm, 542 nm, 554 nm and 561 nm for green emission, respectively. According to the level splitting of Er^{3+} ions in the $Y_3Al_5O_{12}$ crystal reported at [20], the $^4F_{9/2}$ has 5 splitting levels, the $^4S_{3/2}$ has 2 splitting levels and the $^2H_{11/2}$ has 6 splitting levels. So there should have 40 emission wavelengths from the transition of $^4F_{9/2} \rightarrow {}^4I_{15/2}$ ranged from 644 nm to 679 nm, 16 emission wavelengths from the transition of $^4S_{3/2} \rightarrow {}^4I_{15/2}$ ranged from 542 nm to 561 nm and 48 emission wavelengths from the transition of $^4H_{11/2} \rightarrow {}^4I_{15/2}$ ranged from 516 nm to 539 nm. As mentioned above, the thermal vibration of crystal lattice at room temperature makes the assignment for a specific transition impossible.

From Fig. 8, the integral emission intensity of core-shell sample and pure $Y_3Al_5O_{12}$ powders is calculated to be 6562 and 44038 from $^4F_{9/2}$, 2652 and 13045 from $^2H_{11/2}$, 29657 and 170189 from $^4S_{3/2}$ to the ground state, respectively. One can note that the integral intensity emitted from $^4S_{3/2}$ is ten times more than that from $^2H_{11/2}$. It stems from the effect of temperature on the population [22]. In addition, the integral intensity of the green emission is five times more than that of the red emission, which means that the ESA 2 and ET 2 processes dominates the ESA 1 and ET 1 processes in the $Y_3Al_5O_{12}:Er^{3+}$.

The effect of the coating cycles on the upconversion luminescence has the same tendency as the downconversion luminescent emission mentioned above. It is also noted that the $SiO_2@Y_3Al_5O_{12}:Er^{3+}$ sample has a finger upconversion pattern, which is similar with that of the pure $Y_3Al_5O_{12}:Er^{3+}$ powders and different from that of glass, further confirming that Er^{3+} ions of core-shell sample are located at the ordered crystal structure. Moreover, the stronger upconversion emission of the $SiO_2@Y_3Al_5O_{12}:Er^{3+}$ sample makes it have a potential use as an upconversion fluorescent nanobioprobe in replacement of the commonly-used downconversion fluorescent nanobioprobes, which suffer from autofluorescence, photo-damage to living organisms and less tissue penetration under the ultraviolet (UV) excitation [23].

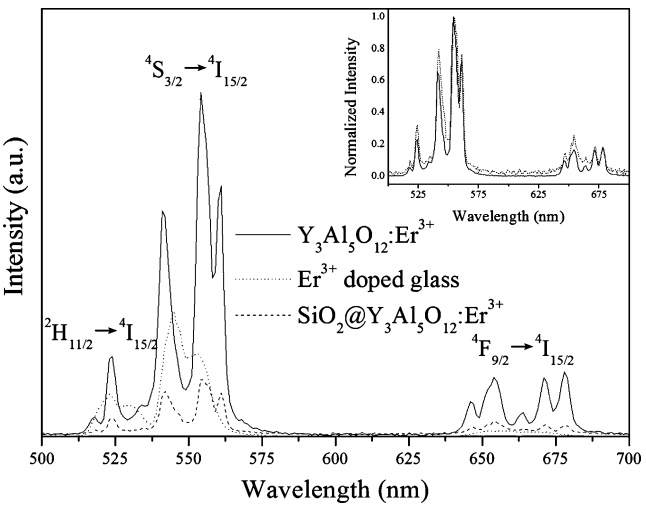

Fig. 8 Upconversion luminescent spectra of the $SiO_2@Y_3Al_5O_{12}:Er^{3+}$, $Y_3Al_5O_{12}:Er^{3+}$ powders and Er^{3+} doped glass in visible region. The inset is the normalization spectra of the $SiO_2@Y_3Al_5O_{12}:Er^{3+}$ and $Y_3Al_5O_{12}:Er^{3+}$ samples, respectively

Conclusions

The core-shell structure $SiO_2@Y_3Al_5O_{12}:Er^{3+}$ powders were synthesized with a simple modified Pechini-Type sol-gel method. The obtained particles preserved the spherical morphology, sub-micrometer size and a narrow size distribution. Upon the excitation of 980 nm LD, the luminescence spectra of the core-shell powders are similar to those of the pure $Y_3Al_5O_{12}:Er^{3+}$ powders except the intensity, indicating that Er^{3+} ions of core-shell sample are located at the ordered crystal structure. Downconversion and upconversion emission are observed simultaneously at room temperature with the excitation of 980-nm LD, which demonstrates that the $SiO_2@Y_3Al_5O_{12}:Er^{3+}$ powders can be used as phosphors in bio-probe researches.

Acknowledgements This work is financially supported by the GSTP (Grant No.2006Z2-D0161), GSTP (Grant No.2006J1-C0491) and NSFC (Grant No.50602017).

Reference

1. Masayuki N, Setsuhisa T, Masashi I, Masaru T, Koji F, Kazuyuki H (2005) Optical-telecommunication -band fluorescence properties of Er^{3+}-doped YAG nanocrystals synthesized by glycothermal method. Opt. Mater 27:655–662 doi:10.1016/j.optmat.2004.08.074
2. Liu M, Wang SW, Zhang J, An LQ, Chen LD (2007) Dominant red emission $\left({}^4F_{9/2} \rightarrow {}^4I_{15/2}\right)$ via upconversion in YAG $(Y_3Al_5O_{12}):Yb^{3+}$, Er^{3+} nanopowders. Opt. Mater 29:1352–1357 doi:10.1016/j.optmat.2006.03.028
3. Ann S (1994) Upconversion excitation of green fluorescence in Er:YAG. J. Lumin 60–61:636–9
4. Georgescu S, Toma O, Ivanov I (2005) Upconversion from the ${}^4I_{13/2}$ and ${}^4I_{11/2}$ levels in Er:YAG. J. Lumin 114:43–52 doi:10.1016/j.jlumin.2004.11.009
5. Gruber JB, Quagliano JR, Reid MF, Richardson FS, Hils ME, Seltzer MD, Stevens SB, Morrison CA, Allik TH (1993) Energy levels and correlation crystal-field effects in Er^{3+}-doped garnets. Phys Rev B 48:15561–15573 doi:10.1103/PhysRevB.48.15561
6. Matkovskii AO, Sugak DY, Durygin AN, Kaczmarek S, Kopczyñski K, Mierczyk Z, Lukasiewicz T, Shakhov AP (2005) Effect of ionizing radiation on optical and lasing properties of $Y_3Al_5O_{12}$ single crystals doped with Nd, Er, Ho, Tm, Cr ions. Opt. Mater 6:353–358 doi:10.1016/S0925-3467(96)00049-3
7. Gruber JB, Nijjar AS, Sardar DK, Yow RM, Russel CC III, Allik TH, Zandi B (2005) Spectral analysis and energy-level structure of $Er^{3+}(4f^{11})$ in polycrystalline ceramic garnet $Y_3Al_5O_{12}$. J Appl Phys 97:063519 doi:10.1063/1.1861148
8. Sardar DK, Russel CC III, Gruber JB, Allik TH (2005) Absorption intensities and emission cross section of principal intermanifold and inter-Stark transitions of $Er^{3+}(4f^{11})$ in polycrystalline ceramic garnet $Y_3Al_5O_{12}$. J Appl Phys 97:123501 doi:10.1063/1.1928327
9. Jia PY, Liu MX, Li GZ (2006) Sol–gel synthesis and characterization of $SiO_2@CaWO_4$, $SiO_2@CaWO_4:Eu^{3+}/Tb^{3+}$ core–shell structured spherical particles. Nanotechnology 17:734–742 doi:10.1088/0957-4484/17/3/020
10. Lin CK, Li YY, Yu M, Yang PP, Lin J (2007) A facile synthesis and characterization of monodispersed spherical pigment particles with a core/shell structure. Adv Funct Mater 17:1459–1465 doi:10.1002/adfm.200600775
11. Schärtl W (2000) Crosslinked spherical nanoparticles with core-shell topology. Adv Mater 12:1899–1908 doi:10.1002/1521-4095(200012)12:24<1899::AID-ADMA1899>3.0.CO;2-T
12. Giaume D, Buissette V, Lahlil K, Gacoin T, Boilot JP, Casanova D, Beaurepaire E, Sauviat MP, Alexandrou A (2005) mission properties and applications of nanostructured luminescent oxide nanoparticles. Prog Solid State Chem 33:99–106 doi:10.1016/j.progsolidstchem.2005.11.041
13. Zhong CJ, Maye MM (2001) Core-shell assembled nanoparticles as catalysts. Adv Mater 13:1507–1511 doi:10.1002/1521-4095(200110)13:19<1507::AID-ADMA1507>3.0.CO;2-#
14. Liu XM, Lin J (2007) Synthesis and characterization of monodispersed spherical core-shell structured $SiO_2@Y_3Al_5O_{12}:Ce^{3+}/Tb^{3+}$ phosphors for field emission displays. J Nanopart Res 9:869–875 doi:10.1007/s11051-006-9146-x
15. Hreniak D, Psuja P, Strek W, Hölsä J (2008) Luminescence properties of $Y_3Al_5O_{12}:Eu^{3+}$-coated submicron SiO_2 particles. J Non-Cryst Sollids 354:445–450
16. Stöber W, Fink A, Bohn EJ (1968) Controlled growth of monodisperse silica spheres in the micron size range. J Colloid Interface Sci 26:62–69 doi:10.1016/0021-9797(68)90272-5
17. Zhang JH, Zhan P, Wang ZL (2003) Preparation of monodisperse silica particles with controllable size and shape. J Mater Res 18:649–653 doi:10.1557/JMR.2003.0085
18. Pechini MP (1967) US Patent no.3330697
19. Liu XM, Jia PY, Lin J, Li GZ (2006) Monodisperse spherical core-shell structured SiO_2-$CaTiO_3:Pr^{3+}$ phosphors for field emission displays. J Appl Phys 99:124902 doi:10.1063/1.2204751
20. Kaminskii AA, Butaeva TI, Fedorov VA, Bagdasarov KS, Petrosyan AG (1977) Absorption, luminescence, and stimulated emission investigations in $Lu_3Al_5O_{12}$-Er^{3+} crystals. phys stat sol (a) 39:541–48
21. Xiao K, Yang ZM, Feng ZM (2007) Upconversion luminescence mechanisms of Er^{3+}-doped barium gallogermanate glasses. Acta Phys Sin 56:3178–3184 in Chinese
22. Yu YQ, Wu ZJ, Zhang SY (2000) Concentration effects of Er^{3+} ion in YAG:Er laser crystals. J Alloy Comp 302:204–208 doi:10.1016/S0925-8388(99)00630-1
23. Lim SF, Riehn R, Ryu WS, Khanarian N, Tung CK, Tank D, Austin RH (2006) In vivo and scanning electron microscopy imaging of upconverting nanophosphors in caenorhabditis elegans. Nano Lett 6:169–174 doi:10.1021/nl0519175